

Hyper-Rayleigh scattering from CH₄, CD₄, CF₄, and CCl₄

Robby D. Pyatt and David P. Shelton^{a)}

Department of Physics, University of Nevada, Las Vegas, Las Vegas, Nevada 89154-4002

(Received 22 February 2001; accepted 20 March 2001)

First hyperpolarizabilities β were obtained for CX₄ molecules in gas and liquid phases from hyper-Rayleigh scattering measurements at $\lambda = 1064$ nm. The gas-phase results for β_{xyz} (atomic units) are 7.1 ± 0.9 (CH₄), 7.0 ± 0.9 (CD₄), 5.4 ± 0.6 (CF₄), and 11.0 ± 0.9 (CCl₄). *Ab initio* calculations of β are consistent with the experimental results for CF₄ and CCl₄, but not for CH₄ and CD₄. The effective liquid-phase β for CCl₄ is $3 \times$ the gas phase value, but the liquid environment has little effect on β for the other molecules. Thermal-lens and absorption coefficients were also measured for ten liquids. © 2001 American Institute of Physics. [DOI: 10.1063/1.1370941]

I. INTRODUCTION

Recently, dynamic first hyperpolarizabilities β for CH₄, CF₄, and CCl₄ were calculated by Bishop, Gu, and Cybulski.¹ The initial motivation for this calculation was to compare with an experimental β value for CCl₄ proposed as a standard for hyper-Rayleigh scattering (HRS) measurements,² and CH₄ and CF₄ were included when it was recognized that there were little experimental or theoretical data for these molecules. The initial motivation for the present work was to test these calculations for CH₄, CF₄, and CCl₄. These molecules are small enough that high quality *ab initio* calculations are feasible, so a critical comparison with experiment would be interesting. Quantitatively accurate *ab initio* quantum chemical calculations of dynamic molecular hyperpolarizabilities are still difficult despite great advances in computational power, since they require a large basis set and a high-level treatment of electron correlation, which must include frequency dependence, and must account for both electronic and vibrational degrees of freedom.^{3,4} Assessing the accuracy of the calculated results can pose a problem since it is usually not feasible to exhaustively address all computational issues simultaneously, and because there are few accurate gas-phase experimental results for comparison.

Two attractive simplifications for tetrahedral (T_d) CX₄ molecules are that the tensor β has only one independent component β_{xyz} , and calculation of a single bond length determines the equilibrium geometry. Since the dipole moment is zero, HRS is the only experimental technique suitable for measuring β for these molecules. HRS has recently become one of the principal methods for measuring the nonlinear optical properties of molecules in solution,^{5,6} but very few measurements have been made in the gas phase. The first gas in which HRS was observed was CH₄, at $\lambda = 694.3$ nm by Maker in 1966.^{7,8} However, his experimental value for β is uncertain by a factor of 3,⁷ and no other measurement for CH₄ exists. The only other gas-phase measurement of β for one of these molecules is the recent experimental result for CCl₄ at $\lambda = 1064$ nm,² which disagrees with

the *ab initio* calculation of Bishop *et al.*¹ by about a factor of 2. The main goal of the present work is to obtain reliable experimental measurements of β for CH₄, CD₄, CF₄, and CCl₄ in the gas phase for comparison with *ab initio* calculations. HRS measurements were also made for liquid CH₄, CD₄, CF₄, and CCl₄ to investigate the effects of intermolecular interactions on the nonlinear optical properties of these molecules in the condensed phase.

II. HRS EXPERIMENT

The experimental apparatus and methods used in this work have been previously described,^{2,9} and a detailed description of the present experiment can be found in Ref. 10. The beam from a pulsed Nd:YAG laser operating at $\lambda = 1064$ nm was focused into a liquid or gas sample contained in a 1 cm fused silica fluorimeter cuvette, and the scattered light near $\theta = 90^\circ$ and $\lambda = 532$ nm was collected with an $f/1.8$ lens and analyzed by a grating spectrometer with calibrated spectral response. The incident beam in the sample had a waist diameter ≈ 15 μm , and the pulses typically had a 1.5 kHz repetition rate, ≈ 100 ns duration and ≈ 0.7 mJ energy. A visible-blocking glass filter (Schott RG-850) placed just before the laser focusing lens prevented second-harmonic light generated along the beam path from entering the sample region. The polarization of the incident laser beam was controlled using a prism polarizer and a Soleil-Babinet compensator, while the polarization of the collected light was analyzed using a sheet polarizer followed by a quartz wedge polarization scrambler. The polarization geometry was VV, with both the incident and the detected scattered polarization perpendicular to the scattering plane, except for two gas-phase measurements in which the analyzer was removed to increase the signal by measuring VV+VH.⁹ The spectrometer slits were opened as large as possible (25 cm^{-1} spectral slit width) to maximize the HRS signal and to minimize the sensitivity to shifts in alignment. Gated photon counting detection was used, giving a typical gated photomultiplier dark count rate of 2×10^{-4} counts/s (cps). The peak HRS signals were ≈ 100 cps for the room temperature liquid samples, ≈ 0.1 cps for the cryogenic liquids, and $\approx 2 \times 10^{-3}$ cps for gas-phase samples. Dead-time corrections^{9,11} were signifi-

^{a)}Electronic mail: shelton@physics.unlv.edu

cant only for the room temperature liquid HRS signals. Alignment of the sample cell and optics was done with a room temperature liquid in the cuvette, and when the sample was changed the dependence of image position on sample refractive index was compensated by precalculated displacements of the focusing and collection lenses.⁹ Multiple scans over the selected spectral region were made for each measurement. Intensity was recorded at $\approx 1 \text{ cm}^{-1}$ intervals, although the data is displayed using bins as coarse as 12 cm^{-1} .

Several different sample cells were used. For CH_3CN and CCl_4 vapor samples a standard Teflon-stoppered cuvette was used. The cuvette was filled with 1 cm^3 of reagent-grade liquid passed through a $0.2 \mu\text{m}$ micropore filter, and placed in a thermostatic enclosure heated to $50\text{--}75 \text{ }^\circ\text{C}$ to give a gas mixture composed of air and 380–730 Torr of vapor above the liquid surface. The major constituents of air have no dipole-allowed SHG, and the presence of air as a buffer gas is thought to suppress some types of background problems. The pressure and density of the vapor were determined from the measured liquid temperature.^{12,13} For CH_4 , CD_4 , and CF_4 gas samples a cuvette with a graded-seal glass stem connected to a gas shut-off valve was used. The cuvette was cleaned, connected to a gas-handling manifold, evacuated and outgassed, filled with ultrahigh purity gas through a $0.5 \mu\text{m}$ sintered metal dust filter to a typical pressure of 3000 Torr (4 atm), and then sealed and removed from the manifold. The gas density was determined from the measured fill pressure and temperature¹³ (there was no significant uncertainty in the gas density during the HRS measurements due to leaks). Liquid CCl_4 at room temperature ($22 \text{ }^\circ\text{C}$) in a standard stoppered cuvette was the intensity reference for the gas and vapor HRS measurements.

Cryogenic liquid CH_4 , CD_4 , and CF_4 samples were held in a different graded-seal cuvette. This cuvette was suspended inside a top-loading optical cryostat by its glass stem, and remained connected to the manifold during the HRS measurements. To prepare the sample, sample gas was condensed into a Pyrex glass reservoir tube on the manifold and then vacuum distilled into the cuvette which was typically held at 100 K. The vapor pressure and temperature of the sample were continuously monitored and were used to determine the density of the liquid.^{12,14–20} The intensity reference for the cryogenic liquid HRS measurements was liquid CH_3CN at 295 K in the same cuvette (liquid CCl_4 was the reference for a single measurement). To prepare the reference, liquid CH_3CN in a second reservoir tube on the manifold was degassed by freeze/pump/thaw cycles and then vacuum distilled into the cuvette. Each time CH_3CN was removed from the cell, prolonged pumping was required to desorb solvent vapor absorbed by the rubber O-ring seals on the connection to the sample cell. An advantage of filling the cell by vacuum distillation was that disturbances of the sample cell position between sample and reference measurements were minimized.

The gated random background was easily and accurately measured and was much smaller than the peak HRS signal even for the gas phase measurements. More problematic was background due to sources synchronized in time with the laser pulses. Synchronous background sources observed in

the gas-phase measurements included incandescent dust particles and two-photon fluorescence. The signal from a dust particle, incinerated as it passes through the laser beam focus, is a short burst with a flat spectrum. This background was reduced by carefully cleaning the sample cell, filtering the gas, pressurizing the sample cell slowly, and allowing time for dust to settle before starting the measurement. The two-photon fluorescence signal from contaminants on the cell surface was also spectrally flat over the 600 cm^{-1} region probed, but steady in time. This background was eliminated by careful cleaning and handling of the sample cell. A type of background observed only for CCl_4 vapor and not fully understood, was sporadic bursts with no discernable spectral dependence, which were brighter and more persistent than the bursts for dust. A possible explanation is two-photon fluorescence from products of a gas-phase chemical reaction initiated by incineration of a dust particle; the signal fades as the reaction products are removed by dissolving into the reservoir of liquid CCl_4 . Careful cleaning of the cuvette eliminated this background.

Several methods were used to assess the synchronous background, and any measurement with a large synchronous background was discarded. Synchronous background can be distinguished from HRS by observations made far from line center, or by filling the sample cell with N_2 gas for which there is no dipole-allowed HRS. Synchronous background contributions from dust could also be identified by time dependence of the signal or by statistically improbable fluctuations in the signal. No single method was used for every measurement or gave conclusive results alone. Every run and sometimes even single scans were separately inspected for synchronous background contributions. The synchronous background contribution for the measurements used in the final analysis was 4%–9% of the integrated intensity for the gases and 0% for the liquids.

III. THERMAL LENS

Absorption of the 1064 nm laser beam by molecular vibration overtones causes localized heating and a decrease in the refractive index of the liquid along the beam path. The result is a negative lens distributed along the laser beam path in the liquid, which modifies the propagation of the laser beam (the effect is negligibly weak in the gases studied). The effects of the thermal lens are an increase in the focal spot size and a decrease in the HRS signal, and these depend on the sample composition and laser power. To extract molecular properties from the HRS signals, it is necessary to correct the observed intensities to those that would be seen in the absence of the thermal lens. A simple empirical method to determine the thermal lens correction is to measure I_{HRS}/P^2 as a function of average power P and extrapolate to $P=0$, as previously demonstrated.⁹ This method could not be used for the cryogenic liquids since the HRS signals were too weak at low power to give reliable results. Instead, separate measurements of the thermal lens coefficient of each liquid were made, and the HRS thermal lens correction was calculated. This procedure was tested by comparing the calculated results with direct HRS measurements for liquid CH_3CN .

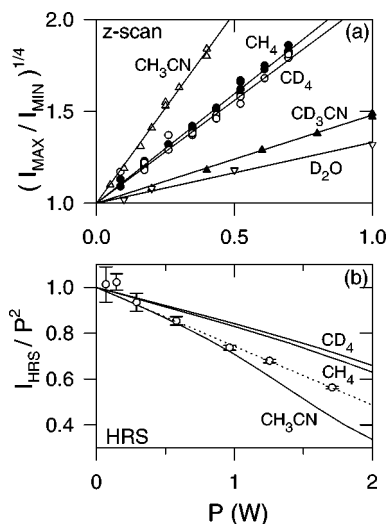


FIG. 1. (a) Z-scan measurements for several liquids at $\lambda = 1064$ nm. For each value of the beam power P , the maximum and minimum values of far field intensity are recorded as the sample in a 1 cm cuvette is scanned along the cw laser beam focused to a confocal parameter $z_0 \approx 5$ mm (beam waist diameter $70 \mu\text{m}$ in the absence of a thermal lens). Fitting Eq. (1) to the intensity ratio gives the thermal lens coefficient A in Table I. (b) Results for I_{HRS}/P^2 vs P , normalized to 1 at $P=0$, are shown. The calculated HRS intensity reduction due to the thermal lens is shown for CH_4 , CD_4 , and CH_3CN by the solid curves. The open circles and the dotted fitted line are the result of experimental measurements for CH_3CN under the same conditions as in the calculation.

Observations of far-field beam profiles were introduced by Sheik-Bahae *et al.* as a sensitive method for measuring nonlinear optical interactions.²¹ Their method, referred to as a “z-scan,” has been adapted here to measure thermal lens strengths in liquids. A focused laser beam passes through the sample cell and falls on a small centered aperture placed in the far field. The central intensity of the beam is measured by a detector placed behind this aperture. As the sample is moved along the beam in the direction of beam propagation, the far-field beam divergence and spot size first reach a minimum as the sample approaches the beam waist, and then reach a maximum as the sample passes the beam waist. The detector signal shows a maximum followed by a minimum as the sample is moved through the focus of the beam. The ratio of maximum to minimum signal is easily measured, and at low power obeys the relation,

$$(I_{\text{max}}/I_{\text{min}})^{1/4} = 1 + AP. \quad (1)$$

TABLE II. Thermal parameters for liquid CH_4 , CD_4 , and CH_3CN used in calculating HRS thermal lens corrections. The estimated uncertainty in the absorption coefficient b is 30%. Values in parentheses for CD_4 assume k and ρc_p are the same as for CH_4 .

Liquid	T (K)	dn/dT (10^{-4}K^{-1})	k^a (10^{-3}W cm^{-1})	ρ (g cm^{-3})	c_p^a ($\text{J g}^{-1} \text{K}^{-1}$)	b (10^{-3}cm^{-1})
CH_4	100	-9.6^b	2.081	0.439 ^c	3.373	0.70
CD_4	100	-9.7^d	(2.08)	0.556 ^d	(2.66)	0.65
CH_3CN	295	-4.5^e	1.877	0.782 ^e	2.227	1.91

^aReference 12.

^bReferences 16, 18, 20.

^cReferences 12, 14, 16, 18–20.

^dReference 16.

^eReference 15.

TABLE I. Thermal lens coefficient A in Eq. (1) measured by z-scan at $\lambda = 1064$ nm for liquids at $T = 28^\circ\text{C}$ (CH_4 and CD_4 at $T = 100$ K). Data for five of the liquids are shown in Fig. 1. The error bars reflect the accuracy of relative comparisons and do not include calibration uncertainties of beam power and focusing. Thermal lens strength is reduced 1–20 \times by deuteration.

Liquid	A (W^{-1})
CH_3OH	40 ± 10
CH_3OD	11 ± 1
H_2O	7 ± 1
CH_3CN	2.07 ± 0.03
CH_4	1.19 ± 0.01
CD_4	1.12 ± 0.02
CD_3CN	0.48 ± 0.01
D_2O	0.33 ± 0.01
CF_4	$< 10^{-2}$
CCl_4	$< 10^{-3}$

Figure 1 and Table I show the results of z-scan measurements made for several liquids with a cw laser beam at $\lambda = 1064$ nm.

The analysis of the z-scan measurements is based on the expression from Gordon *et al.*²² for the steady state thermal lens under conditions of conductive heat transport,

$$f^{-1} = \frac{bP\Delta z}{k\pi r^2} \left(\frac{1}{n} \frac{dn}{dT} \right), \quad (2)$$

where f is the focal length of the thermal lens induced in a liquid layer of small thickness Δz by a Gaussian laser beam with radius r and power P . The relevant material parameters of the liquid are the absorption coefficient b , the thermal conductivity k , and the relative refractive index temperature coefficient $n^{-1}dn/dT$. The thermal lens controlled by conduction is governed by the combination $(b/nk)dn/dT$. The solution for the beam inside the liquid and in the far field was obtained by numerically propagating a Gaussian beam through the sample considered as a series of thin lenses with strength given by Eq. (2). The beam solution calculated using the measured input laser beam parameters is a function of $(b/nk)dn/dT$, so the absorption coefficient b can be determined by fitting the beam propagation calculation to the z-scan measurements and using tabulated material parameters, as shown in Table II for CH_4 , CD_4 , and CH_3CN . A

noteworthy and surprising result is that the measured absorption and thermal lens coefficients are almost the same for CH₄ and CD₄ at $\lambda = 1064$ nm.

The HRS measurements use a pulsed laser beam, which complicates the thermal lens calculation. In the cw limit the temperature distribution is controlled by k , whereas in the limiting case of a single pulse, much shorter than the thermal diffusion time across the beam, the heat capacity ρc_p controls the temperature.²³ The actual situation is intermediate between these two limits. The radial temperature profile and the effective thermal lens at the peak of the laser pulse were obtained from a self-consistent numerical solution of the diffusion equation in cylindrical coordinates with periodic pulsed heat input from the Gaussian beam. The solution for the beam propagating in the presence of the thermal lens, and the integral of I^2 over the sample volume (proportional to the HRS signal), were then calculated as a function of beam power. Figure 1 shows the calculated HRS thermal lens corrections as a function of beam power for CH₄, CD₄, and CH₃CN, as well as experimental results for CH₃CN under the same conditions. The observed deviation between calculated and experimental results for CH₃CN at high power is consistent with the onset of convection,²⁴ which was neglected in the calculation. For CH₄ and CD₄ the calculated results are expected to be more accurate since the thermal lens for a given input power is only half as strong as for CH₃CN, and because convective effects at the same absorbed power will be diminished due to the $8\times$ larger kinematic viscosity of CH₄ and CD₄. The thermal lens corrections for CH₄ and CD₄ were based on the calculated curves in Fig. 1, while the corrections for CH₃CN were based on empirical extrapolation of experimental measurements of I_{HRS}/P^2 . The typical HRS intensity reduction due to the thermal lens in these experiments was 20% for CH₄ and CD₄, and 40% for CH₃CN. The uncertainty in the HRS intensity due to the thermal lens correction was 5% for these three molecules. No correction was needed for CF₄ or CCl₄.

IV. ANALYSIS AND CALIBRATION

The HRS signal is related to the effective molecular hyperpolarizability β by

$$S^{2\omega} \propto \rho G \beta^2, \quad (3)$$

where $S^{2\omega}$ is the HRS signal integrated over the entire spectral band after applying dead time, background, thermal lens, polarization, and spectral response corrections, ρ is the molecular number density, and G accounts for other sample dependent factors, and is given by^{2,9}

$$G = L^4 L_{2\omega}^2 T_{\omega}^2 T_{2\omega} n_{\omega} / n_{2\omega}^2. \quad (4)$$

In this expression n is the sample refractive index,

$$L = (n^2 + 2)/3 \quad (5)$$

is the Lorentz local field factor, and $T = 1 - (n - n_{\text{fs}})^2 / (n + n_{\text{fs}})^2$ is the Fresnel transmission factor for the sample/fused silica (fs) interface. Table III shows ρ and G for the sample materials studied in this work. Relative values of β

TABLE III. Material property data used to determine ρ and G in Eqs. (3) and (4).

Material	T (K)	ρ (mol/l)	n_{ω}	$n_{2\omega}$	G
CH ₄ (l)	100	27.4 ^a	1.276 ^b	1.288 ^b	2.42
CD ₄ (l)	100	27.7 ^b	1.272 ^b	1.284 ^b	2.38
CF ₄ (l)	100	20.7 ^c	1.224 ^d	1.233 ^d	2.01
CCl ₄ (l)	295	10.4 ^e	1.4500 ^f	1.4630 ^f	4.51
CH ₃ CN(l)	295	19.0 ^e	1.3376 ^f	1.3456 ^f	3.02
Gases			1.000	1.000	0.905
Fused silica	295		1.450	1.461	

^aReferences 12, 14, 16, 18–20.

^bReference 16.

^cReferences 12, 14, 17, 19, 20.

^dReferences 17 and 20.

^eReferences 12, 14, 15.

^fReference 15.

are obtained by comparing HRS measurements of $(S^{2\omega}/\rho G)^{1/2}$ from different samples in the same apparatus under nearly identical conditions.

Absolute values of β were obtained using liquid CCl₄ as the intensity standard for the gas measurements, and using liquid CH₃CN as the intensity standard for the liquid measurements. The calibration of these intensity standards is based on the gas-phase β measured for CH₃CN at $\lambda = 1064$ nm in a previous electric-field-induced second harmonic generation (ESHG) experiment.² The calibration chain for the liquid CCl₄ intensity standard is

$$\beta_{\text{ESHG}}^{\text{CH}_3\text{CN}(g)} \Rightarrow \beta_{\text{HRS}}^{\text{CH}_3\text{CN}(g)} \Rightarrow \beta_{\text{HRS}}^{\text{CCl}_4(l)}. \quad (6)$$

The first link of the chain relies on *ab initio* results for ratios of β tensor components.^{2,25} The second link relies on a direct comparison of HRS intensities for CH₃CN gas and CCl₄ liquid. One may consider effective β for liquid CCl₄ as just a convenient way of expressing the HRS scattering cross section measured for the liquid. A final direct comparison of HRS intensities for CH₃CN and CCl₄ liquids also calibrates liquid CH₃CN as an intensity standard. A previous result for $\beta_{\text{HRS}}^{\text{CCl}_4(l)}$ was obtained using several chains of comparisons involving gas- and liquid-phase measurements for seven different molecules,² and the present and previous results are compared in Table IV. The present result for CCl₄ is considered more reliable (and was used in the subsequent analysis) because the signal to noise ratio is better and the synchronous background contributions are more adequately assessed in the present gas-phase HRS measurements.

TABLE IV. Calibration chain for the liquid CCl₄ HRS intensity standard [Eq. (6)]. HRS results are for VV polarization and β is in atomic units.^a

Quantity	Present	Previous
$\beta_{\text{ESHG}}^{\text{CH}_3\text{CN}(g)}$	17.9 ± 1.1 ^b	
$\beta_{\text{HRS}}^{\text{CH}_3\text{CN}(g)}$	10.85 ± 0.68 ^b	
$\beta_{\text{HRS}}^{\text{CCl}_4(l)}$	20.9 ± 1.4	18.6 ± 0.7 ^b

^a $\beta = 1$ a.u. = $1 e^3 a_0^3 E_h^{-2} = 3.20636 \times 10^{-53}$ C³ m³ J⁻² = 8.6392×10^{-33} esu, where e is the electron charge, a_0 is the Bohr radius, and E_h is the Hartree energy.

^bReference 2.

All experimental HRS results are reported for VV polarization geometry. Two gas-phase CF_4 measurements with liquid CCl_4 as the intensity standard were done in the VV+VH polarization geometry. For T_d molecules in the gas phase the HRS depolarization ratio is $S_{\text{VH}}/S_{\text{VV}}=2/3$ by symmetry, while for liquid CCl_4 the measured integrated intensity depolarization ratio was $S_{\text{VH}}/S_{\text{VV}}=0.435$. The VV HRS intensity ratio $S^{\text{CF}_4(\text{g})}/S^{\text{CCl}_4(\text{l})}$ was obtained in this case by multiplying the VV+VH intensity ratio by $(1+0.435)/(1+2/3)$.

The HRS signal given by Eq. (3) in the VV polarization geometry is proportional to $\langle \beta_{\text{ZZZ}}^2 \rangle$, where β_{ZZZ} is the space-fixed ZZZ component of the β tensor and $\langle * \rangle$ denotes the classical average over all molecular orientations.²⁶ The space-fixed components of the orientation-averaged tensor β can be expressed in terms of the tensor components of β in the molecule-fixed frame. For molecules of T_d symmetry β_{xyz} is the only independent component of β , and isotropic averaging for an isolated molecule gives²⁶

$$\langle \beta_{\text{ZZZ}}^2 \rangle = \frac{12}{35} \beta_{\text{xyz}}^2 \quad (7)$$

The HRS signal intensity from a sample of independent, randomly oriented T_d molecules is proportional to the quantity in Eq. (7), but the HRS signal from each individual molecule in the sample fluctuates due to its motion. Orientation diffusion of the molecules results in a Lorentzian HRS band, with spectral width inversely proportional to the orientation diffusion time.²⁷ The integrated intensity of the HRS band is independent of the dynamics, but it is changed by intermolecular interactions and orientation correlations such as those which may exist in a dense liquid. In the gas phase at low density the molecules are independent and freely rotating.

The quantum mechanical view of gas-phase HRS is the process where two incident photons are absorbed, a harmonic photon is scattered and a molecule undergoes a transition between rotational states. The HRS spectrum for a gas of T_d molecules composed of distinguishable atoms consists of seven overlapping branches with line intensities and selection rules given by^{7,28}

$$I_{\text{VV}}^{2\omega}|_{J \rightarrow J'} \propto \beta_{\text{xyz}}^2 (2J+1)(2J'+1) \exp[-BJ(J+1)/kT], \quad (8a)$$

$$\Delta J = 0, \pm 1, \pm 2, \pm 3, \quad (8b)$$

$$J+J' \geq 3, \quad (8c)$$

where B_0 is the rotational constant for the molecule and $B_0J(J+1)$ is the energy of the J rotational level. The spectrum calculation is more complicated and the spectral distribution is less regular in the case of CX_4 molecules with indistinguishable X atoms.^{29–34} To correctly account for nuclear spin statistics and symmetry the molecular states become linear combinations of spherical top rotational wave functions. The partition function is given by Wilson,³⁰ and expressions for the transition matrix elements are given by Ozier and Fox^{31,32} with corrections by Rosenberg *et al.*^{33,34} The full calculation based on symmetry adapted wave functions was used to calculate the HRS spectrum for CH_4 , CD_4 , and CF_4 , but Eq. (8) was used for CCl_4 where isotopic mixing breaks the symmetry. The molecular parameters^{1,35,36}

TABLE V. Parameters for the pure-rotation HRS spectrum calculation, and the calculated quantum corrections to the integrated intensities at $T = 100$ K (295 K). The quantum correction is due to the J dependence of the transition matrix elements. In the absence of nuclear spin statistical effects the quantum correction for CH_4 would increase to 2.0% (1.0%) at 100 K (295 K).

Molecule	Nuclear spin	B_0 (cm^{-1})	Quant. corr. (%)
CH_4	1/2	5.2410 ^a	0.23(0.27)
CD_4	1	2.6326 ^b	0.94(0.57)
CF_4	1/2	0.185 ^c	0.16(0.06)
CCl_4	3/2	0.057 ^d	0.06(0.02)

^aReference 35.

^bReference 36.

^cBased on bond length 0.1320 nm from Ref. 1.

^dBased on bond length 0.1767 nm from Ref. 1.

used in the spectral calculations are shown in Table V. The calculated line spectrum was convolved with the 25 cm^{-1} wide spectrometer spectral response function to obtain the theoretical spectrum, which can be directly compared with the measured HRS spectrum. The effect of nuclear spin statistics on the calculated spectral distribution is significant only for CH_4 and CD_4 , and the quantum corrections to the integrated intensities are negligible for all the molecules. The quantum calculation gives an integrated intensity larger than that obtained using the classical orientation average in Eq. (7), but it agrees with Eq. (7) in the classical limit (large T or small B_0). The calculated quantum corrections are shown in Table V. Theoretical gas-phase HRS spectra were calculated for comparison with each of the measured spectra.

V. RESULTS AND DISCUSSION

The results of the gas-phase HRS measurements are shown in Fig. 2 and Table VI. CH_4 was the first gas studied and also the most difficult case because its HRS signal was the weakest. The CH_4 spectrum shown in Fig. 2 is the sum of 9 measurements with a total of 590 counts above background. The integrated intensity ratio for CH_4 in Table VI is based on the four measurements with the smallest uncertainty in the synchronous background. The synchronous background estimate was $9 \pm 9\%$ of the CH_4 integrated intensity. The envelope of the calculated spectrum agrees with the measured spectral distribution, but not all the peaks in the calculated spectrum appear in the data. The spectrum calculated instead with Eq. (8), ignoring nuclear spin statistical effects, has essentially the same envelope, but is smoother and is a better match to the observed spectrum. The perturbations due to collisions in the CH_4 gas at 4 atm pressure may break the symmetry of the four indistinguishable H atoms, and modify the calculated intensity distribution shown in Fig. 2. Table VI shows that the *ab initio* result for β_{xyz} of CH_4 is 30% larger than the experimental result, well outside the $\pm 13\%$ experimental error bar. The stated theoretical result was obtained by interpolating the tabulated results of Bishop *et al.*,¹ and includes the electronic ($\beta^e = -8.7522$), zero-point vibrational averaging ($\beta^{\text{ZPVA}} = -1.2055$) and pure vibrational ($\beta^v = +0.7541$) contributions at the experimental laser frequency ($9395 \text{ cm}^{-1} = 0.04281 \text{ a.u.}$).

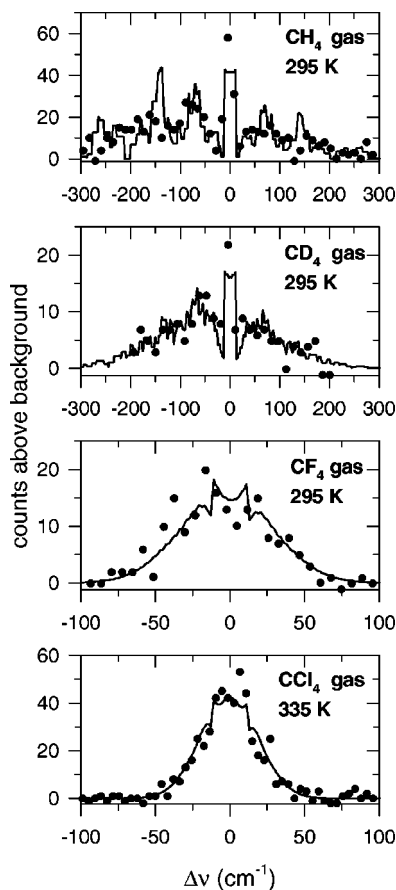


FIG. 2. HRS spectral intensities for CH_4 , CD_4 , CF_4 , and CCl_4 in the gas-phase are plotted vs frequency difference $\Delta\nu$ from the laser second harmonic frequency $2\nu_0 = 18\,790\text{ cm}^{-1}$. The filled circles are the experimental results and the curve is the calculated gas-phase HRS spectrum normalized to match the measured integrated intensity above background. The (random+synchronous) background which was subtracted from the total measured intensity was (3.9 ± 1.2) , (1.9 ± 0.3) , (3.0 ± 0.2) , and (2.1 ± 1.0) counts/point, giving 590, 174, 173, and 501 counts above background for CH_4 , CD_4 , CF_4 , and CCl_4 , respectively. The calculated and measured spectral profiles agree within the statistical uncertainties ($\pm N^{1/2}$ for each point where N is the signal+background count), except for CH_4 where not all the predicted spectral peaks appear in the data.

The results for CD_4 in Fig. 2 and Table VI are from a single good measurement with synchronous background $4 \pm 4\%$ of the integrated intensity. There is good agreement between the calculated and measured spectra over the measured frequency range, and the calculated spectrum was used

TABLE VI. Summary of gas-phase HRS intensity measured with VV polarization, and a comparison of measured and calculated β_{xyz} in atomic units.

Molecule	$\left(\frac{S}{\rho}\right)^{\text{CX}_4(g)} / \left(\frac{S}{\rho}\right)^{\text{CCl}_4(l)}$ (10^{-3})	Measured $ \beta_{xyz} $ (a.u.)	<i>ab initio</i> β_{xyz} (a.u.)
CH_4	8.0 ± 0.9	7.1 ± 0.9	-9.20^a
CD_4	7.8 ± 0.8	7.0 ± 0.9	-9.10^b
CF_4	4.7 ± 0.4	5.4 ± 0.6	4.34^a
CCl_4	22 ± 2	11.0 ± 0.9	$8.7\text{--}13.6^a$

^aFrom Ref. 1.

^bScaled from β for CH_4 from Ref. 1.

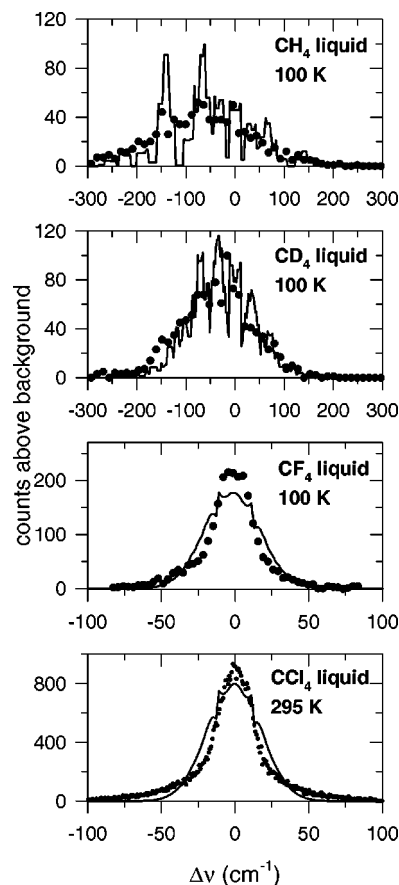


FIG. 3. HRS spectral intensities for CH_4 , CD_4 , CF_4 , and CCl_4 in the liquid-phase are plotted vs frequency difference $\Delta\nu$ from the laser second harmonic frequency $2\nu_0 = 18\,790\text{ cm}^{-1}$. The filled circles are the experimental results and the curve is the calculated gas-phase HRS spectrum at the same temperature, normalized to match the measured integrated intensity above background. The spectra shown are the sum of two measurements for CH_4 and CF_4 , and single measurements for CD_4 and CCl_4 . The measured spectra for CH_4 and CD_4 have the same overall width and shape as the calculated gas-phase spectra but are missing the narrow peaks and valleys. The measured spectra for CF_4 and CCl_4 differ in shape and width from the calculated gas-phase spectra. The experimental spectra have a narrow central peak and low broad wings. When spectrally resolved, the central peak in the liquid CCl_4 spectrum is a Lorentzian with 11.7 cm^{-1} full width at half maximum intensity (Ref. 42).

to estimate the contribution to the integrated intensity for CD_4 due to the clipped tails of the measured spectrum (7%). Table VI shows that the *ab initio* result for β_{xyz} of CD_4 is 30% larger than the experimental result, well outside the $\pm 13\%$ experimental error bar. The theoretical result for CD_4 in Table VI was obtained from the CH_4 results,¹ using the same electronic contribution and scaling the vibrational contributions to β . The assumed scaling is $\beta^{\text{ZPVA}} \propto m^{-1/2}$, $\beta^v \propto \nu_0 / (\nu^2 - \nu_0^2)$ and $\nu_0 \propto m^{-1/2}$, where $\nu_0 = 3100\text{ cm}^{-1}$ for CH_4 was obtained from a fit to the calculated frequency dependence of β^v . The scale factors used are 0.707 for β^{ZPVA} and 0.669 for β^v .

The experimental value of β_{xyz} is 30% smaller than the *ab initio* value for both CH_4 and CD_4 . This is surprising, as the experimental error bars are $\pm 13\%$ and the accuracy of the calculation is thought to be even better. Maroulis thoroughly investigated basis set and correlation effects for β^e in the static limit for CH_4 at the equilibrium geometry,³⁷ as well

TABLE VII. Summary of liquid-phase HRS intensity and effective β measurements with VV polarization. The quantity $w^{(l)}/w^{(g)}$ compares the HRS spectral width measured for the liquid with the calculated width in the gas phase.

Molecule	$\left(\frac{S}{\rho}\right)^{CX_3(l)} / \left(\frac{S}{\rho}\right)^{CH_3CN(l)}$ (10^{-2})	$\left(\frac{S}{\rho}\right)^{CX_3(l)} / \left(\frac{S}{\rho}\right)^{CH_3CN(g)}$	$w^{(l)}/w^{(g)}$	$\beta^{(l)}$ (a.u.)	$\beta^{(l)}/\beta^{(g)}$
CH ₄	1.52 ± 0.03	0.25 ± 0.02	1.1 ± 0.1 ^a	3.3 ± 0.3	0.79 ± 0.09
CD ₄	1.63 ± 0.05	0.28 ± 0.02	1.1 ± 0.1 ^a	3.4 ± 0.3	0.84 ± 0.09
CF ₄	0.74 ± 0.02	0.122 ± 0.007	0.4 ± 0.1 ^b	2.5 ± 0.2	0.80 ± 0.09
CCl ₄	90 ± 3	18.4 ± 0.8	0.29 ± 0.03 ^c	20.9 ± 1.4	3.0 ± 0.1

^aRoot-mean-square width (RMS).

^bFull width at half maximum height (FWHM) after deconvolution of the instrumental width.

^cFWHM of the Lorentzian component of the resolved liquid spectrum from Ref. 42 compared with the calculated resolved gas spectrum.

as the sensitivity to bond length. Comparing static $\beta^e = -8.31$ a.u. from Maroulis' work³⁷ and -8.09 a.u. from Bishop *et al.*¹ suggests that β^e at the laser frequency from Bishop *et al.* has converged within 0.3 a.u. The β^{ZPV^A} and β^v terms should be comparably accurate, so one expects accuracy near 4% for *ab initio* β for CH₄ (and CD₄). A possible explanation for the discrepancy between theory and experiment is that the β^v calculation includes only the fundamental vibrations, and relatively low order overtone and combination vibration bands of CH₄ and CD₄ that fall near the laser frequency have been ignored. Such vibration bands close to the laser frequency are seen in the gas-phase³⁸ and solid-phase^{39,40} absorption spectra for CH₄ and CD₄. The effect of near-resonant overtone and combination bands below the laser frequency will be to reduce the magnitude of calculated β and decrease the discrepancy between theory and experiment. The required overtone vibration contribution to β^v is 2 a.u., larger than the fundamental contribution. If the transition matrix elements are $\approx 30\times$ smaller than for the fundamentals, the transition frequencies would have to lie within ≈ 300 cm⁻¹ of the laser frequency to have the desired effect. Since the downward shifts in the vibration frequencies between CH₄ and CD₄ are large, it might seem unlikely that the same large resonant contribution to β^v would exist for both molecules. For the same reason one expects the absorption coefficient to be much smaller for CD₄ than for CH₄. However, the observed fact is that the absorption coefficients are almost the same for CH₄ and CD₄ at the laser frequency, and the same accident may have occurred for β^v . This issue could be resolved theoretically by calculating the overtone and combination band contributions to β^v , or experimentally by measuring β at visible wavelengths where all contributions to β^v are far from resonance.

The results for CF₄ and CCl₄ in Fig. 2 and Table VI combine five and four measurements, with synchronous background contributions $5 \pm 5\%$ and $9 \pm 9\%$ of the integrated intensity, respectively. There is good agreement between the measured and calculated spectra in Fig. 2. The *ab initio* result shown in Table VI for β_{xyz} of CF₄ is 1.1 a.u. smaller than the experimental result. However, comparison of the results from Bishop *et al.*¹ with the static *ab initio* results from Maroulis⁴¹ suggests that extending the basis set and level of correlation treatment could increase *ab initio* β

in Table VI for CF₄ by 1.6 a.u. Thus, the experimental value 5.4 ± 0.6 a.u. for β_{xyz} of CF₄ falls within the range of the best *ab initio* estimates, 4.3–5.9 a.u. Similarly for CCl₄, the lower *ab initio* value given in Table VI is calculated using a uniform basis set and correlation treatment for all contributions to β , while the higher value includes estimates of the effects of extending the basis set and level of correlation treatment. The range of the best *ab initio* results for β_{xyz} for CCl₄ includes the experimental value from this work. The present experimental result for β_{xyz} of CCl₄ in the gas phase is smaller by almost a factor of 2 than the previously reported result.² The most likely source of the discrepancy is an unrecognized synchronous background contribution in the previous measurements. In this regard one may note that the largest synchronous background contributions have been observed for CCl₄ vapor, and for this reason special care has been taken in the present work to assess and minimize this background.

The results of the liquid-phase HRS measurements are shown in Fig. 3 and Table VII. The background in the liquid spectra was usually <1% of the integrated intensity. The $\beta^{(l)}$ results for liquid CH₄, CD₄, and CF₄ in Table VII are based on four, one, and two measurements, respectively, calibrated against liquid CH₃CN. The $\beta^{(l)}$ result for liquid CCl₄ in Tables IV and VII is based on seven measurements calibrated directly against CH₃CN gas. Figure 3 shows that the pronounced rotational structure of the gas-phase CH₄ and

TABLE VIII. Parameters for estimating intermolecular interaction effects, in atomic units.

Molecule	Ω^a (a.u.)	γ^b (10^3 a.u.)	$(\gamma\Omega/\beta)^2$ (10^6 a.u.)	Ω^2 (a.u.)
CH ₄	+2.41 ^c	3.324 ^d	1.3	5.8
CF ₄	-4.66 ^e	1.54 ^f	1.8	21.7
CCl ₄	22.3 ^g	19.7 ^h	1600	497

^a $\Omega = 1$ a.u. = $1 e a_0^3 = 2.374 182 \times 10^{-50}$ C m³.

^b $\gamma = 1$ a.u. = $1 e^4 a_0^4 E_h^{-3} = 6.235 378 \times 10^{-65}$ C⁴ m⁴ J⁻³.

^cReference 37.

^dStatic γ from Ref. 43.

^eReference 41.

^fKerr effect γ at $\lambda = 632.8$ nm from Ref. 44.

^gReference 45.

^hKerr effect γ at $\lambda = 632.8$ nm from Ref. 46.

CD₄ HRS spectra calculated at the temperature of the cryogenic liquids, is absent from the experimental liquid HRS spectra. The measured width of the liquid spectrum for CH₄ and CD₄, however, is not significantly different from the width of the calculated gas-phase spectrum, as shown in Fig. 3 and Table VII. This indicates that the intermolecular interactions in liquid CH₄ and CD₄ only weakly perturb the rotational motion. In contrast, the CF₄ and CCl₄ liquid HRS spectra are significantly narrowed compared to the calculated gas-phase spectra at the same temperature, as shown in Fig. 3 and Table VII. Theory predicts that the free rotor HRS spectrum collapses to a narrow Lorentzian profile as the rotational motion becomes strongly hindered.²⁷ The large HRS intensity in the case of CCl₄ allows high resolution measurements⁴² which show that the liquid HRS spectrum is 3 times narrower than the gas-phase spectrum, indicating strongly hindered rotation in liquid CCl₄.

The ratio $\beta^{(l)}/\beta^{(g)}$ in Table VII is a measure of the effect of intermolecular interactions on β . Both molecular distortion and orientation correlation will change the value of effective $\beta^{(l)}$ that is measured. Only CCl₄ shows a large deviation from $\beta^{(l)}/\beta^{(g)} = 1$. This can be understood by considering the multipolar interactions for these molecules. The octupole moment Ω is the first nonzero multipole moment for these molecules. The octupolar electric field of a molecule, $\propto \Omega R^{-5}$, will distort any nearby molecule, inducing a time-varying increment $\Delta\beta(R) \propto \gamma \Omega R^{-5}$ during a collision. The intermolecular field fluctuates on the collisional time scale ≈ 0.3 ps, so the relevant γ is the static value (which contains a large vibrational contribution). Collision-induced distortion results in the addition of broad exponential wings to the HRS spectrum, with added integrated intensity $\propto \gamma^2 \Omega^2$. These collision-induced exponential wings have been previously studied, contribute 40% of the integrated intensity for CCl₄,⁴² and are clearly visible in the liquid CCl₄ HRS spectrum shown in Fig. 3. Theory predicts that the relative collision-induced HRS contribution is $\propto (\gamma \Omega / \beta)^2$. The value of $(\gamma \Omega / \beta)^2$ estimated using the molecular parameters^{37,41-46} given in Table VIII is 1000× larger for CCl₄ than for the other molecules, consistent with observation of significant collision-induced HRS only for liquid CCl₄. The second effect of Ω is to exert intermolecular torques $\propto \Omega^2 R^{-5}$ during collisions, which hinder free rotation of the molecules and induce orientation correlation. The results are a narrowing of the rotational HRS spectrum and a change in the measured effective $\beta^{(l)}$. Table VIII shows that Ω^2 is at least 20× times larger for CCl₄ than for the other molecules, consistent with observation of strongest spectral narrowing due to hindered rotation for liquid CCl₄, and suggesting that orientation correlation effects will be most significant for CCl₄. Orientation correlation may account for the small deviation from $\beta^{(l)}/\beta^{(g)} = 1$ observed for CH₄, CD₄, and CF₄.

VI. CONCLUSION

Contrary to expectations, the agreement between experimental and calculated results for β is poor for CH₄ and CD₄. The discrepancy may be due to β^v contributions from near-

resonant overtone vibrations. For CF₄ and CCl₄ the gas-phase experimental results for β fall within the range of the best *ab initio* results. The results for β measured in liquid CH₄, CD₄, and CF₄ are consistent with weak intermolecular interactions.

ACKNOWLEDGMENTS

The authors thank Lisa Hsu for her help with the cryogenic liquid HRS measurements. This work was supported in part by the U.S. Army Research Office under Grant No. G-DAAD19-99-1-0086.

- ¹D. M. Bishop, F. L. Gu, and S. M. Cybulski, *J. Chem. Phys.* **109**, 8407 (1998).
- ²P. Kaatz, E. A. Donley, and D. P. Shelton, *J. Chem. Phys.* **108**, 849 (1998).
- ³D. M. Bishop, *Adv. Quantum Chem.* **25**, 1 (1994).
- ⁴D. M. Bishop, in *Advances in Chemical Physics*, edited by I. Prigogine and S. A. Rice (Wiley, New York, 1998), Vol. 104, p. 1.
- ⁵K. Clays and A. Persoons, *Phys. Rev. Lett.* **66**, 2980 (1991).
- ⁶K. Clays, A. Persoons, and L. de Maeyer, in *Modern Nonlinear Optics, Advances in Chemical Physics*, edited by I. Prigogine and S. A. Rice (Wiley, New York, 1994), Vol. 85, part 3, p. 455.
- ⁷P. D. Maker, in *Physics of Quantum Electronics*, edited by P. L. Kelly, B. Lax, and P. E. Tannenwald (McGraw-Hill, New York, 1966), p. 60.
- ⁸J. F. Verdieck, S. H. Peterson, C. M. Savage, and P. D. Maker, *Chem. Phys. Lett.* **7**, 219 (1970).
- ⁹P. Kaatz and D. P. Shelton, *Rev. Sci. Instrum.* **67**, 1438 (1996).
- ¹⁰R. D. Pyatt, M.S. thesis, University of Nevada, Las Vegas, 2001.
- ¹¹D. P. Shelton, *Phys. Rev. A* **42**, 2578 (1990).
- ¹²*CRC Handbook of Thermophysical and Thermochemical Data*, edited by D. R. Lide and H. V. Kehianian (CRC Press, Boca Raton, FL, 1994).
- ¹³J. H. Dymond and E. B. Smith, *The Virial Coefficients of Gases and Mixtures* (Clarendon, Oxford, 1980).
- ¹⁴N. B. Vargaftik, Y. K. Vinogradov, and V. S. Yargin, *Physical Properties of Liquids and Gases*, 3rd ed. (Begell, New York, 1996).
- ¹⁵J. Timmermans, *Physico-Chemical Constants of Pure Organic Compounds* (Elsevier, New York, 1950), Vols. 1 and 2.
- ¹⁶A. Yoshihara, A. Anderson, R. A. Aziz, and C. C. Lim, *Chem. Phys.* **48**, 183 (1980).
- ¹⁷A. Yoshihara, A. Anderson, R. A. Aziz, and C. C. Lim, *Chem. Phys.* **51**, 141 (1980).
- ¹⁸J. D. Olson, *J. Chem. Phys.* **63**, 474 (1975).
- ¹⁹M. J. Terry, J. T. Lynch, M. Bunclark, K. R. Mansell, and L. A. K. Staveley, *J. Chem. Thermodyn.* **1**, 413 (1969).
- ²⁰C. P. Abbiss, C. M. Knobler, R. K. Teague, and C. J. Pings, *J. Chem. Phys.* **42**, 4145 (1965).
- ²¹M. Sheik-Bahae, A. A. Said, T. Wei, D. J. Hagan, and E. W. Van Stryland, *IEEE J. Quantum Electron.* **26**, 760 (1990).
- ²²J. P. Gordon, R. C. C. Leite, R. S. Moore, S. P. S. Porto, and J. R. Whinnery, *J. Appl. Phys.* **36**, 3 (1965).
- ²³M. C. Gupta, S. D. Hong, A. Gupta, and J. Moacanin, *Appl. Phys. Lett.* **37**, 505 (1980).
- ²⁴A. Bejan, *Heat Transfer* (Wiley, New York, 1993).
- ²⁵M. Stahelin, C. R. Moylan, D. M. Burland, A. Willetts, J. E. Rice, D. P. Shelton, and E. A. Donley, *J. Chem. Phys.* **98**, 5595 (1993).
- ²⁶R. Bersohn, Y. H. Pao, and H. L. Frisch, *J. Chem. Phys.* **45**, 3184 (1966).
- ²⁷P. D. Maker, *Phys. Rev. A* **1**, 923 (1970).
- ²⁸K. Altmann and G. Strey, *J. Raman Spectrosc.* **12**, 1 (1982).
- ²⁹G. Herzberg, *Molecular Spectra and Molecular Structure. II. Infrared and Raman Spectra of Polyatomic Molecules* (Van Nostrand, Princeton, 1955).
- ³⁰E. B. Wilson, *J. Chem. Phys.* **3**, 276 (1935).
- ³¹I. Ozier and K. Fox, *J. Chem. Phys.* **52**, 1416 (1970).
- ³²K. Fox and I. Ozier, *J. Chem. Phys.* **52**, 5044 (1970).
- ³³A. Rosenberg and I. Ozier, *J. Chem. Phys.* **65**, 418 (1976).
- ³⁴A. Rosenberg and J. Susskind, *Can. J. Phys.* **57**, 1081 (1979).
- ³⁵D. L. Gray and A. G. Robiette, *Mol. Phys.* **32**, 1607 (1976).
- ³⁶S. Brodersen, D. L. Gray, and A. G. Robiette, *Mol. Phys.* **34**, 617 (1977).
- ³⁷G. Maroulis, *Chem. Phys. Lett.* **226**, 420 (1994).
- ³⁸A. R. W. McKellar, *Can. J. Phys.* **67**, 1027 (1989).

- ³⁹P. Calvani, S. Cunsolo, S. Lupi, and A. Nucara, *J. Chem. Phys.* **96**, 7372 (1992).
- ⁴⁰P. Calvani, A. Nucara, M. C. Salvasaggio, and S. Lupi, *J. Chem. Phys.* **101**, 20 (1994).
- ⁴¹G. Maroulis, *Chem. Phys. Lett.* **259**, 654 (1996).
- ⁴²P. Kaatz and D. P. Shelton, *Mol. Phys.* **88**, 683 (1996).
- ⁴³D. M. Bishop and S. P. A. Sauer, *J. Chem. Phys.* **107**, 8502 (1997).
- ⁴⁴D. P. Shelton and J. J. Palubinskas, *J. Chem. Phys.* **104**, 2482 (1996).
- ⁴⁵I. R. Dagg, M. Missio, A. Anderson, W. Smith, and L. A. A. Read, *Can. J. Phys.* **67**, 507 (1989).
- ⁴⁶M. P. Bogaard, B. J. Orr, A. D. Buckingham, and G. L. D. Ritchie, *J. Chem. Soc., Faraday Trans. 2* **74**, 1573 (1978).